spectra are plotted as a function of the difference between the laser photon energy $\hbar\omega_p$ and the emission photon energy $\hbar\omega_l$. A number of sharp peaks labeled c, e, f, g, i and j are observed depending on the excitation energy. Their positions correspond to the separation between the ground and excited states of the neutral acceptors. The peaks c and e are assigned to Li acceptors while the remaining peaks are identified with Na acceptors. Their widths are now determined by homogeneous broadening only. From these selectively excited DAP spectra, *Tews* et al. [7.52] have determined accurately the binding energy and excited state energies of Na and Li acceptors in ZnSe.

7.2 Light Scattering Spectroscopies

Although most of the light traveling through a medium is either transmitted or absorbed following the standard laws of reflection and refraction (which obtain from $\boldsymbol{k}$-conservation), a very tiny fraction is scattered, in all directions, by inhomogeneities inside the medium. These inhomogeneities may be static or dynamic. Defects such as dislocations in a crystal are static scatterers and scatter the light elastically (i. e., without frequency change). Fluctuations in the density of the medium that are associated with atomic vibrations are examples of dynamic scatterers. Other examples of scattering mechanisms in semiconductors are fluctuations in the charge or spin density. Inelastic scattering of light by acoustic waves was first proposed theoretically by *Brillouin* [7.53] and later independently by *Mandelstam* [7.54]. Inelastic scattering of light by molecular vibrations was first reported by *Raman* [7.55]. In 1930 *Raman* was awarded the Nobel prize for his discovery of Raman scattering. Today Raman scattering and resonant Raman scattering have become standard spectroscopic tools in the study of semiconductors. In this section we shall first present a macroscopic theory of Raman scattering by phonons in solids. This is followed by a microscopic theory and a discussion of resonant Raman scattering. The rest of the section is devoted to discussions of Brillouin scattering by acoustic modes and *resonant Brillouin scattering* by exciton-polaritons.

7.2.1 Macroscopic Theory of Inelastic Light Scattering by Phonons

Consider an infinite medium with electric susceptibility χ. As shown in Sect. 6.1, the electrical susceptibility should be a second rank tensor in general. For the time being we shall assume the medium to be isotropic so that χ can be represented by a scalar. When a sinusoidal plane electromagnetic field described by

$$\boldsymbol{F}(\boldsymbol{r},t) = \boldsymbol{F}_i(\boldsymbol{k}_i,\omega_i)\cos(\boldsymbol{k}_i\cdot\boldsymbol{r}-\omega_i t) \tag{7.27}$$

is present in this medium, a sinusoidal polarization $\boldsymbol{P}(\boldsymbol{r},t)$ will be induced:

$$\boldsymbol{P}(\boldsymbol{r},t) = \boldsymbol{P}(\boldsymbol{k}_\mathrm{i},\omega_\mathrm{i})\cos(\boldsymbol{k}_\mathrm{i}\cdot\boldsymbol{r}-\omega_\mathrm{i}t). \tag{7.28}$$

Its frequency and wavevector are the same as those of the incident radiation while its amplitude is given by

$$\boldsymbol{P}(\boldsymbol{k}_\mathrm{i},\omega_\mathrm{i}) = \chi(\boldsymbol{k}_\mathrm{i},\omega_\mathrm{i})\boldsymbol{F}_\mathrm{i}(\boldsymbol{k}_\mathrm{i},\omega_\mathrm{i}). \tag{7.29}$$

If the medium is at a finite temperature there are fluctuations in χ due to thermally excited atomic vibrations. We have seen in Chap. 3 that the normal modes of atomic vibrations in a crystalline semiconductor are quantized into phonons. The atomic displacements $\boldsymbol{Q}(\boldsymbol{r},t)$ associated with a phonon can be expressed as plane waves:

$$\boldsymbol{Q}(\boldsymbol{r},t) = \boldsymbol{Q}(\boldsymbol{q},\omega_0)\cos(\boldsymbol{q}\cdot\boldsymbol{r}-\omega_0 t) \tag{7.30}$$

with wavevector $\boldsymbol{q}$ and frequency ω_0. These atomic vibrations will modify χ. We assume that the characteristic electronic frequencies which determine χ are much larger than ω_0, hence χ can be taken to be a function of $\boldsymbol{Q}$. This is known as the quasi-static or adiabatic approximation. Normally the amplitudes of these vibrations at room temperature are small compared to the lattice constant and we can expand χ as a Taylor series in $\boldsymbol{Q}(\boldsymbol{r},t)$:

$$\chi(\boldsymbol{k}_\mathrm{i},\omega_\mathrm{i},\boldsymbol{Q}) = \chi_0(\boldsymbol{k}_\mathrm{i},\omega_\mathrm{i}) + (\partial\chi/\partial\boldsymbol{Q})_0\boldsymbol{Q}(\boldsymbol{r},t) + \ldots, \tag{7.31}$$

where χ_0 denotes the electric susceptibility of the medium with no fluctuations. The second term in (7.31) represents an oscillating susceptibility induced by the lattice wave $\boldsymbol{Q}(\boldsymbol{r},t)$. Substituting (7.31) into (7.29) we can express the polarization $\boldsymbol{P}(\boldsymbol{r},t,\boldsymbol{Q})$ of the medium in the presence of atomic vibrations as

$$\boldsymbol{P}(\boldsymbol{r},t,\boldsymbol{Q}) = \boldsymbol{P}_0(\boldsymbol{r},t) + \boldsymbol{P}_\mathrm{ind}(\boldsymbol{r},t,\boldsymbol{Q}), \tag{7.32}$$

where

$$\boldsymbol{P}_0(\boldsymbol{r},t) = \chi_0(\boldsymbol{k}_\mathrm{i},\omega_\mathrm{i})\boldsymbol{F}_\mathrm{i}(\boldsymbol{k}_\mathrm{i},\omega_\mathrm{i})\cos(\boldsymbol{k}_\mathrm{i}\cdot\boldsymbol{r}-\omega_\mathrm{i}t) \tag{7.33}$$

is a polarization vibrating in phase with the incident radiation and

$$\boldsymbol{P}_\mathrm{ind}(\boldsymbol{r},t,\boldsymbol{Q}) = (\partial\chi/\partial\boldsymbol{Q})_0\boldsymbol{Q}(\boldsymbol{r},t)\boldsymbol{F}_\mathrm{i}(\boldsymbol{k}_\mathrm{i},\omega_\mathrm{i})\cos(\boldsymbol{k}_\mathrm{i}\cdot\boldsymbol{r}-\omega_\mathrm{i}t) \tag{7.34}$$

is a polarization wave induced by the phonon (or other similar fluctuation). Polarization waves can also be induced indirectly by longitudinal optical (LO) phonons via their macroscopic electric fields (Sect. 6.4). For the time being we shall neglect this effect.

To determine the frequency and wavevector of $\boldsymbol{P}_\mathrm{ind}$ we rewrite $\boldsymbol{P}_\mathrm{ind}(\boldsymbol{r},t,\boldsymbol{Q})$ as

$$\begin{aligned}\boldsymbol{P}_\mathrm{ind}(\boldsymbol{r},t,\boldsymbol{Q}) &= (\partial\chi/\partial\boldsymbol{Q})_0\boldsymbol{Q}(\boldsymbol{q},\omega_0)\cos(\boldsymbol{q}\cdot\boldsymbol{r}-\omega_0 t)\\ &\quad\times\boldsymbol{F}_i(\boldsymbol{k}_\mathrm{i},\omega_i)\cos(\boldsymbol{k}_\mathrm{i}\cdot\boldsymbol{r}-\omega_\mathrm{i}t) \qquad (7.35\mathrm{a})\\ &= \tfrac{1}{2}(\partial\chi/\partial\boldsymbol{Q})_0\boldsymbol{Q}(\boldsymbol{q},\omega_0)\boldsymbol{F}_\mathrm{i}(\boldsymbol{k}_\mathrm{i},\omega_\mathrm{i}t)\\ &\quad\times\{\cos[(\boldsymbol{k}_\mathrm{i}+\boldsymbol{q})\cdot\boldsymbol{r}-(\omega_\mathrm{i}+\omega_0)t] \qquad (7.35\mathrm{b})\\ &\quad+\cos[(\boldsymbol{k}_\mathrm{i}-\boldsymbol{q})\cdot\boldsymbol{r}-(\omega_\mathrm{i}-\omega_0)t]\}\,.\end{aligned}$$

$\boldsymbol{P}_{\text{ind}}$ consists of two sinusoidal waves: a *Stokes* shifted wave with wavevector $\boldsymbol{k}_{\text{S}} = (\boldsymbol{k}_{\text{i}} - \boldsymbol{q})$ and frequency $\omega_{\text{S}} = (\omega_{\text{i}} - \omega_0)$ and an *anti-Stokes* shifted wave with wavevector $\boldsymbol{k}_{\text{AS}} = (\boldsymbol{k}_{\text{i}} + \boldsymbol{q})$ and frequency $\omega_{\text{AS}} = (\omega_i + \omega_0)$.

The radiation produced by these two induced polarization waves is known, respectively, as **Stokes scattered** and **anti-Stokes scattered** light. Since the phonon frequency is equal to the difference between the incident photon frequency ω_{i} and the scattered photon frequency ω_{s}, this difference is referred to as the **Raman frequency** or **Raman shift** (one also speaks of **Stokes** and **anti-Stokes shifts**). Raman spectra are usually plots of the intensity of the scattered radiation versus the Raman frequency.

When compared to nonlinear optical spectroscopy, light scattering can be regarded as a kind of *parametric process*, since it involves periodically changing a parameter (namely, the electrical susceptibility) of the medium. However, the change induced is bilinear in the phonon displacement and the electric field and therefore light scattering is not a nonlinear optical process as are optical parametric processes.[2] The phonon modulation of the susceptibility at frequency ω_0 generates sidebands at frequencies $\omega_{\text{i}} \pm \omega_0$ to the incident radiation at frequency ω_{i}. In this respect light scattering resembles *frequency modulation* (FM) in radio transmission. The incident radiation plays the role of the *carrier wave*.

Notice that *both frequency and wavevector are conserved in the above scattering processes*. As a result of wavevector conservation, the wavevector q of phonons studied by one-phonon Raman scattering must be smaller than twice the photon wavevector. Assuming that visible lasers are used to excite Raman scattering in a sample with refractive index about 3, q is of the order of $10^6\ \text{cm}^{-1}$. This value is about 1/100 of the size of the Brillouin zone in a semiconductor. Hence *one-phonon Raman scattering probes only zone-center phonons*. In such experiments q can usually be assumed to be zero.

The expansion in (7.31) can be easily extended to second or even higher orders in the phonon displacements. The second-order terms give rise to induced polarizations whose frequencies are shifted from the laser frequency by the amount $\pm\omega_{\text{a}} \pm \omega_{\text{b}}$ (where $\omega_{\text{a}} > \omega_{\text{b}}$ are the frequencies of the two phonons involved). These induced polarizations give rise to **two-phonon Raman scattering**. For two different phonons, peaks with Raman frequencies $\omega_{\text{a}} + \omega_{\text{b}}$ and $\omega_{\text{a}} - \omega_{\text{b}}$ are referred to as the **combination** and **difference modes**, respectively. If the two phonons are identical, the resultant two-phonon Raman peak is called an **overtone**. Wavevector conservation in two-phonon Raman scattering is satisfied when $\boldsymbol{q}_{\text{a}} \pm \boldsymbol{q}_{\text{b}} \approx 0$, where $\boldsymbol{q}_{\text{a}}$ and $\boldsymbol{q}_{\text{b}}$ are the wavevectors of the two phonons a and b, respectively. In overtone scattering this condition implies $\boldsymbol{q}_{\text{a}} = -\boldsymbol{q}_{\text{b}}$, i. e., the two phonons have equal and opposite wavevectors. Thus in two-phonon Raman scattering there is no restriction on the magnitudes of the *individual* phonon wavevectors as there is in one-phonon scattering (only their sum must be near zero). Hence the *overtone* Raman spectrum, after di-

[2] Stimulated Raman scattering (see pp. 258 and 395) however, is a nonlinear optical process.

viding the Raman frequency by two, is a measure of the phonon density of states, although modified by a factor dependent on the phonon occupancy and the scattering efficiency.

For Raman scattering with highly monochromatic x-rays, one cannot assume that $q \approx 0$. In fact, scattering wavevectors sweeping the whole BZ can be obtained by varying the angle between the $\boldsymbol{k}$'s of incident and scattered photons. See [3.7] and [3.28b].

7.2.2 Raman Tensor and Selection Rules

The intensity of the scattered radiation can be calculated from the time-averaged power radiated by the induced polarizations $\boldsymbol{P}_{\text{ind}}$ into unit solid angle. Since the induced polarizations for Stokes and anti-Stokes scattering differ only in their frequencies and wavevectors, we will restrict ourselves to Stokes scattering. This intensity will depend on the polarization of the scattered radiation, $\boldsymbol{e}_{\text{s}}$, as $|\boldsymbol{P}_{\text{ind}} \cdot \boldsymbol{e}_{\text{s}}|^2$. If we denote the polarization of the incident radiation as $\boldsymbol{e}_{\text{i}}$, the scattered intensity I_{s} calculated from (7.35) is proportional to

$$I_{\text{s}} \propto |\boldsymbol{e}_{\text{i}} \cdot (\partial\chi/\partial\boldsymbol{Q})_0 \boldsymbol{Q}(\omega_0) \cdot \boldsymbol{e}_{\text{s}}|^2. \tag{7.36}$$

In (7.36) we have approximated $\boldsymbol{q}$ by zero for one-phonon scattering and allowed for the possibility of χ being complex. Notice that the scattered intensity is proportional to the vibration amplitude $\boldsymbol{Q}$ squared. In other words, there will be no Stokes scattering if no atomic vibration is present. This result is a consequence of our classical treatment. Once we quantize the vibrational modes into phonons, in Stokes scattering, where a phonon is excited in the medium by the incident radiation, the intensity becomes proportional to $(N_q + 1)$, where N_q is the phonon occupancy. (the summand 1 in $N_q + 1$ corresponds to the zero-point motion mentioned, in connection with photons, in Sect. 7.1). Similarly, the anti-Stokes intensity will be proportional to N_q and vanish at low temperatures.

Let us assume that $\boldsymbol{Q}$ is the vector displacement of a given atom induced by the phonon so that $(\partial\chi/\partial\boldsymbol{Q})$ is a third-rank tensor with complex components. By introducing a unit vector $\hat{\boldsymbol{Q}} = \boldsymbol{Q}/|\boldsymbol{Q}|$ parallel to the phonon displacement we can define a complex second rank tensor $\mathcal{R}$ as

$$\mathcal{R} = (\partial\chi/\partial\boldsymbol{Q})_0 \hat{\boldsymbol{Q}}(\omega_0) \tag{7.37}$$

such that I_{s} is proportional to

$$I_{\text{s}} \propto |\boldsymbol{e}_{\text{i}} \cdot \mathcal{R} \cdot \boldsymbol{e}_{\text{s}}|^2. \tag{7.38}$$

$\mathcal{R}$ is known as the **Raman tensor**. In general $\mathcal{R}$ is obtained by a contraction of $\boldsymbol{Q}$ and the derivative of χ with respect to $\boldsymbol{Q}$, and therefore it is a second-rank tensor with complex components like χ.

By measuring the dependence of the scattered intensity on the incident and scattered polarizations one can deduce the symmetry of the Raman tensor and hence the symmetry of the corresponding Raman-active phonon. Thus *Raman scattering can be used to determine both the frequency and symmetry of a zone-center phonon mode*. By means of two-phonon Raman scattering, phonon densities of states can also be estimated. Obviously, Raman scattering is a very powerful tool for studying vibrational modes in a medium. Later in this chapter we shall show that, in addition to studying atomic vibrations, resonant Raman scattering can be used to study interband electronic transitions, excitons, and even electron–phonon interactions. It is also useful to study magnetic excitations [7.56]. Thus Raman scattering is truly one of the most versatile spectroscopic techniques for studying not only semiconductors but also other condensed media.

At first sight, the Raman tensor as defined in (7.37) appears to be a symmetric second-rank tensor, since the susceptibility is a symmetric tensor. This is only exactly correct if we can neglect the slight difference in frequency between the incident and scattered radiation. We shall come back to this point later in this section. Within this approximation, antisymmetric components in the Raman tensor can be introduced only by magnetic fields [7.56]. Since most semiconductors are nonmagnetic we can usually assume the Raman tensor in semiconductors to be symmetric. Additional requirements are often imposed on Raman tensors as a result of the symmetries of the medium and of the vibrational modes involved in the scattering. The result of these symmetry requirements is that the scattered radiation vanishes for certain choices of the polarizations $\boldsymbol{e}_\mathrm{i}$ and $\boldsymbol{e}_\mathrm{s}$ and scattering geometries. These so-called **Raman selection rules** are very useful for determining the symmetry of Raman-active phonons.

The simplest example of Raman selection rules can be found in centrosymmetric crystals. In these crystals phonons can be classified as having even or odd parity under inversion. Since the crystal is invariant under inversion, its tensor properties, such as $(\partial\chi/\partial\boldsymbol{Q})$, should remain unchanged under the same operation. On the other hand, the phonon displacement vector $\boldsymbol{Q}$ of an odd-parity phonon changes sign under inversion, implying that $(\partial\chi/\partial\boldsymbol{Q})$ changes sign. Hence *the Raman tensor of odd-parity phonons in centrosymmetric crystals (within the approximation that the phonon wavevector is zero) must vanish*. As we have seen in Sect. 6.4, these odd-parity phonons can be infrared active while the even-parity phonons cannot. Thus infrared absorption and Raman scattering are complementary in centrosymmetric crystals. In some crystals there are phonon modes which are neither infrared nor Raman active. These phonons are said to be *silent*.

As another example we shall consider Raman selection rules in the zinc-blende-type semiconductor GaAs. Its zone-center optical phonon has symmetry Γ_4 (also called Γ_{15}) as discussed in Sect. 3.1. This is a triply degenerate representation whose three components can be denoted as X, Y, and Z. In this particular case we can regard these three components as equal to the projections of the relative displacement of the two atoms in the unit cell along the crystallographic axes. As we showed in Chap. 3 a third-rank tensor in the zinc-blende

crystal, such as the piezoelectric or the electromechanical tensor, has only one linearly independent and nonzero component, namely, the component with indices xyz and its cyclic permutations, such as yzx, zxy, etc. Thus the third-rank tensor $\partial\chi/\partial\boldsymbol{Q}$ has only one linearly independent component, which we shall denote by d. The nonzero components of the corresponding Raman tensor are dependent on the phonon displacement. For an optical phonon polarized along the x direction, its Raman tensor $\mathcal{R}(X)$ will have only two nonzero components: $\mathcal{R}_{yz}(X) = \mathcal{R}_{zy}(X) = d$. We can represent $\mathcal{R}(X)$ as a 3×3 matrix:

$$\mathcal{R}(X) = \begin{bmatrix} 0 & 0 & 0 \\ 0 & 0 & d \\ 0 & d & 0 \end{bmatrix}. \tag{7.39a}$$

Using similar arguments we can derive the Raman tensors for the equivalent optical phonons polarized along the y and z axes as

$$\mathcal{R}(Y) = \begin{bmatrix} 0 & 0 & d \\ 0 & 0 & 0 \\ d & 0 & 0 \end{bmatrix} \quad \text{and} \quad \mathcal{R}(Z) = \begin{bmatrix} 0 & d & 0 \\ d & 0 & 0 \\ 0 & 0 & 0 \end{bmatrix}. \tag{7.39b}$$

We should keep in mind that the zone-center optical phonon in GaAs is split into a doubly degenerate transverse optical (TO) mode and a longitudinal optical (LO) mode for $q \neq 0$. The Raman tensor elements for these two phonons are different because the LO mode can scatter light via its macroscopic longitudinal electric field (Sect. 6.4). In order to distinguish them we shall use d_{TO} and d_{LO} in their respective Raman tensors.

Using the Raman tensors defined in (7.39) we can now derive the selection rules for Raman scattering in GaAs. Since these selection rules are dependent on the scattering geometry, we shall introduce a notation for describing scattering geometries which can be specified by four vectors: $\boldsymbol{k}_{\mathrm{i}}$ and $\boldsymbol{k}_{\mathrm{s}}$ (the directions of the incident and scattered photons, respectively) and $\boldsymbol{e}_{\mathrm{i}}$ and $\boldsymbol{e}_{\mathrm{s}}$ (the polarizations of the incident and scattered photons, respectively). These four vectors define the scattering configurations usually represented as $\boldsymbol{k}_{\mathrm{i}}(\boldsymbol{e}_{\mathrm{i}}, \boldsymbol{e}_{\mathrm{s}})\boldsymbol{k}_{\mathrm{s}}$.[3]

EXAMPLE: Raman Selection Rule for Backscattering from the (100) Surface of a GaAs Crystal

Since GaAs is opaque to the usual visible laser light (bandgap 1.52 eV at 4 K, see Table 6.3) the simplest scattering geometry is the backscattering one, i. e., $\boldsymbol{k}_{\mathrm{i}}$ and $\boldsymbol{k}_{\mathrm{s}}$ are antiparallel to each other. In order to conserve wavevector, the $\boldsymbol{q}$ of the phonon must be along the [100] direction also for backscattering from a (100) surface. The polarization of a TO phonon must be perpendicular to $\boldsymbol{q}$ (or the x-axis) and therefore its Raman tensor is a linear combination of $\mathcal{R}(Y)$ and $\mathcal{R}(Z)$. The nonzero components of both tensors in (7.39b) dictate that either $\boldsymbol{e}_{\mathrm{i}}$ or $\boldsymbol{e}_{\mathrm{s}}$ must have a projection along the x-axis. If $\boldsymbol{k}_{\mathrm{i}}$ and $\boldsymbol{k}_{\mathrm{s}}$ are both parallel to the x-axis, then $\boldsymbol{e}_{\mathrm{i}}$ and $\boldsymbol{e}_{\mathrm{s}}$ are both perpendicular to

[3] This notation is due to S.P.S. Porto, a Brazilian pioneer of light scattering in semiconductors

Table 7.2. Raman selection rules for backscattering geometries in zinc-blende-type crystals. d_{TO} and d_{LO} denote the non-zero Raman tensor elements for the TO and LO phonons, respectively. y' and z' denote the [011] and [0$\bar{1}$1] axes, while x'', y'' and z'' denote the set of three mutually perpendicular [111], [1$\bar{1}$0] and [11$\bar{2}$] axes (see Problem 7.4)

Scattering geometry	Selection rule	
	TO phonon	LO phonon
$x(y,y)\bar{x}$; $x(z,z)\bar{x}$	0	0
$x(y,z)\bar{x}$; $x(z,y)\bar{x}$	0	$\lvert d_{LO}\rvert^2$
$x(y',z')\bar{x}$; $x(z',y')\bar{x}$	0	0
$x(y',y')\bar{x}$; $x(z',z')\bar{x}$	0	$\lvert d_{LO}\rvert^2$
$y'(x,x)\bar{y}'$	0	0
$y'(z',x)\bar{y}'$	$\lvert d_{TO}\rvert^2$	0
$y'(z',z')\bar{y}'$	$\lvert d_{TO}\rvert^2$	0
$x''(z'',z'')\bar{x}''$	$(2/3)\lvert d_{TO}\rvert^2$	$(1/3)\lvert d_{LO}\rvert^2$
$x''(z'',y'')\bar{x}''$	$(2/3)\lvert d_{TO}\rvert^2$	0

the x-axis, and therefore Raman scattering by the TO phonon is forbidden in this backscattering geometry. For the LO phonon the situation is different since its $\boldsymbol{q}$ is along the x-axis. Its Raman tensor is given by $\mathcal{R}(X)$ instead. For the scattering geometries $x(y,z)\bar{x}$ or $x(z,y)\bar{x}$ the corresponding scattered intensity is proportional to $|d_{LO}|^2$. On the other hand, the LO phonon is forbidden in the geometries $x(y,y)\bar{x}$ and $x(z,z)\bar{x}$. One can also show that the LO phonon is forbidden in the geometries $x(y',z')\bar{x}$ and $x(z',y')\bar{x}$ but allowed in the geometries $x(y',y')\bar{x}$ and $x(z',z')\bar{x}$, where y' and z' denote the [011] and [0$\bar{1}$1] axes, respectively. These and other additional Raman selection rules for backscattering from zinc-blende-type crystals are summarized in Table 7.2. The derivations of these selection rules and the corresponding ones for other scattering geometries are left as an exercise (Problem 7.4).

The general problem of deriving the symmetry of Raman tensors in crystals can be solved with the help of group theory. Again we shall use simple examples as illustrations. The rigorous derivations and discussions can be found in articles by *Loudon* [7.57, 58]. Let us consider again a cubic crystal. We have already shown in Sect. 3.3.1 that a symmetric second rank tensor, like the strain tensor, can be decomposed into three components transforming according to the irreducible representations Γ_1, Γ_3 and Γ_4. Similarly, we expect that the Raman tensor in a zinc-blende crystal can be decomposed into three (irreducible) tensors: $\mathcal{R}(\Gamma_1)$, $\mathcal{R}(\Gamma_3)$ and $\mathcal{R}(\Gamma_4)$. The tensors corresponding to the three irreducible components of Γ_4 have been given in (7.39) already. The Raman tensors belonging to the other two irreducible representations can be derived in the same way as for the strain tensors $e_{ij}(\Gamma_1)$ and $e_{ij}(\Gamma_3)$ in Sect. 3.3.1:

$$\mathcal{R}(\Gamma_1) = \begin{bmatrix} a & 0 & 0 \\ 0 & a & 0 \\ 0 & 0 & a \end{bmatrix} \tag{7.40}$$

$$\mathcal{R}(\Gamma_3) = \begin{bmatrix} b & 0 & 0 \\ 0 & b & 0 \\ 0 & 0 & -2b \end{bmatrix}; \quad \sqrt{3} \begin{bmatrix} b & 0 & 0 \\ 0 & -b & 0 \\ 0 & 0 & 0 \end{bmatrix}. \tag{7.41}$$

While there are no *optical* phonons belonging to these irreducible representations in crystals such as GaAs, these tensor components can be found in two-phonon Raman spectra (to be shown for Si in the next section).

The quantity often measured in a scattering experiment is the **scattering efficiency** η. This can be defined as the ratio of the energy of electromagnetic waves scattered per unit time divided by the energy of incident electromagnetic modes crossing the scattering area per unit time. Using the expression (see, e. g., [7.29]) for the power radiated by the induced dipole in (7.35) we can derive the following expression for η [7.59]:

$$\eta = (\omega_s/c)^4 VL|\boldsymbol{e}_i \cdot (\partial\chi/\partial\boldsymbol{Q})_0 \boldsymbol{Q}(\omega_0) \cdot \boldsymbol{e}_s|^2. \tag{7.42}$$

In (7.42) L is the **scattering length**. If the sample is transparent to the incident light, L is equal to the thickness of the sample along the path of the incident light. Otherwise L is equal to $(\alpha_i + \alpha_s)^{-1}$, where α is the absorption coefficient. V, equal to AL (A being the area of the incident beam), is the volume of the sample producing the scattered radiation. Sometimes the efficiency is defined per unit scattering length L and denoted as S. Notice that η depends on the fourth power of ω_s. Thus short-wavelength light is scattered more efficiently than long-wavelength radiation. This important property of light scattering is responsible for the blue color of the sky on a sunny day and the red sunset. The scattering process in these cases is known as **Rayleigh scattering** and results either from entropy fluctuations or, more commonly these days, from pollutants.

One deficiency of the classical treatment of light scattering presented so far is that the way the atomic displacement associated with the phonon is included in (7.42) which applies only to stimulated emission or absorption of a phonon. It does not work when the phonon is emitted spontaneously in the light scattering process since the value of Q is zero at zero temperature. To rectify this deficiency we use the results of Sects. 5.2 and 7.1. In Sect. 5.2.4 we have stated that the probability of an electron emitting (or absorbing) a phonon with wave vector $\boldsymbol{q}$ is proportional to $N_{\boldsymbol{q}} + 1$ (or $N_{\boldsymbol{q}}$) where $N_{\boldsymbol{q}}$ is the phonon occupation number (p. 126). In Sect. 7.1 we have separated the total light emission rate into two parts: a spontaneous and a stimulated component. The rate of stimulated emission in (7.3) is proportional to the photon energy density. By the same argument we expect the rate of stimulated emission of a phonon to be proportional to the phonon occupation number. Thus since we have defined (7.42) to be the scattering efficiency for a single phonon, the corresponding efficiency for Stokes and Anti-Stokes scattering by $N_{\boldsymbol{q}}$ phonons can be obtained by multiplying (7.42) by the factors $(N_{\boldsymbol{q}} + 1)$ and $N_{\boldsymbol{q}}$, respectively. This result suggests that it may be possible to determine $N_{\boldsymbol{q}}$, and the temperature, from the ratio of the Stokes to Anti-Stokes intensities in Raman scattering.

Another deficiency is that radiation fields are not explicitly quantized into photons. Raman scattering should be regarded as the inelastic scattering of *photons* by quantized excitations in a medium. The efficiency of scattering of particles is usually defined in terms of a **scattering cross section** σ. Let the *flux* of the incident photon beam be N_i photons *per unit area* (A). If N_s is the total number of particles integrated over all directions (or 4π solid angle) and all scattered frequencies, then σ is defined by[4]

$$N_\mathrm{s} = N_\mathrm{i}\sigma. \tag{7.43}$$

Clearly σ has the dimensions of an area. In experiments one usually collects only photons scattered into a cone (with solid angle $\delta\Omega$) pointing in a specific direction and within a scattered frequency range $\delta\omega_\mathrm{s}$ centered on ω_s. In such cases the ratio between the number of scattered photons and the incident photon flux is known as the **differential scattering cross section** $d^2\sigma/d\Omega\, d\omega_\mathrm{s}$. It is related to the second derivative of the scattering efficiency in (7.42) by

$$\frac{d^2\eta}{d\Omega\, d\omega_\mathrm{s}} = \left(\frac{\omega_\mathrm{i}}{\omega_\mathrm{s}A}\right)\left(\frac{d^2\sigma}{d\Omega\, d\omega_\mathrm{s}}\right) \tag{7.44}$$

We stated earlier that the Raman tensor is symmetric with respect to interchange between its two subindices because the electric susceptibility tensor $\chi(\omega)$, from which it is derived, has such symmetry in the limit where the photon wave vectors are negligible [see (6.1)]. This is not strictly correct. $\chi(\omega)$ depends on the photon frequency ω only, while the Raman tensor involves two slightly different frequencies: ω_i and ω_s. *The Raman tensor is symmetric only when we neglect the small difference between* ω_i *and* ω_s. We can derive the correct result, without neglecting this difference, by using **time-reversal symmetry**.

Let us assume that a beam of N_i photons with frequency ω_i and polarization $\boldsymbol{e}_\mathrm{i}$ is incident on a unit area of a medium. The discussion in the rest of this section will refer to a unit volume of sample and per unit time, unless otherwise stated. This beam is Stokes scattered in the medium as shown in Fig. 7.19a. the polarization of the scattered beam is $\boldsymbol{e}_\mathrm{s}$ and its frequency ω_s. The total number of spontaneously scattered photons (i.e., in spontaneous emission discussed in Sect. 7.1; detailed discussion of this point will be postponed until Sect. 7.2.4) will be proportional to $|\boldsymbol{e}_\mathrm{i}\cdot\mathcal{R}(\omega_\mathrm{i},\omega_\mathrm{s})\cdot\boldsymbol{e}_\mathrm{s}|^2 N_\mathrm{i}$. Let us denote the cross section corresponding to $|\boldsymbol{e}_\mathrm{i}\cdot\mathcal{R}(\omega_\mathrm{i},\omega_\mathrm{s})\cdot\boldsymbol{e}_\mathrm{s}|^2$ as $\sigma(\omega_\mathrm{i},\omega_\mathrm{s})$. Thus the number of scattered photons N_s is equal to $\sigma(\omega_\mathrm{i},\omega_\mathrm{s})N_\mathrm{i}$ as long as the number of scattered photons is small and *stimulated* scattering (as in stimulated emission) can be neglected. Notice that the scattering cross section is a scalar quantity defined in terms of photons. However, it can be calculated from the tensor $\mathcal{R}$ defined for macroscopic electromagnetic fields. The arguments in $\sigma(\omega_\mathrm{i},\omega_\mathrm{s})$ serve as

[4] The cross section for scattering of a particle by another particle is uniquely defined. In the case of a solid, however, it depends on the volume under consideration, i.e., a primitive cell, a crystallographic unit cell, 1 cm^3, etc.

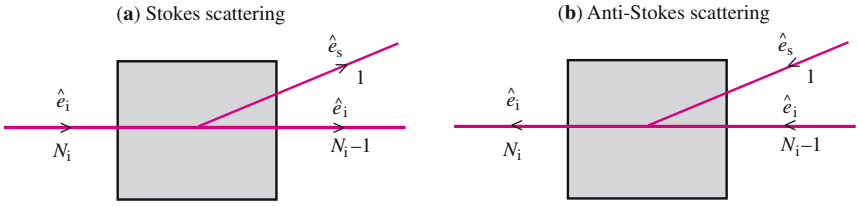

Fig. 7.19. Schematic diagram of (**a**) a Stokes Raman scattering process in a medium and (**b**) its time-reversed anti-Stokes process

reminders of the tensor components in $\mathcal{R}$ from which σ can be derived. Let us assume that the incident photon flux is such that only one scattered photon is produced (Fig. 7.19a). This is equivalent to having

$$N_i = 1/\sigma(\omega_i, \omega_s). \tag{7.45a}$$

The flux of the unscattered beam is therefore $N_i - 1$. In Fig. 7.19b we reverse the direction of time so that the outgoing beams in Fig. 7.19a now become the incoming beams and vice versa. We denote by N_s the total number of photons emerging from unit area of the medium with frequency ω_i. This beam contains $N_i - 1$ photons, which are the unscattered photons. We can neglect loss of photons from this beam due to scattering since it requires at least N_i photons to produce one scattered photon. In addition to these unscattered photons there is an anti-Stokes scattered photon from the single incoming photon with polarization $\boldsymbol{e}_s$ and frequency ω_s. Using the same notation as before for Stokes scattering, the anti-Stokes scattering cross section will be denoted by $\sigma_A(\omega_s, \omega_i)$. Since there are now $N_i - 1$ photons present with the anti-Stokes frequency ω_i we cannot neglect the contribution from stimulated emission. The probability of stimulated emission is proportional to one plus the number of photons present (Sect. 7.1). Therefore the anti-Stokes scattered photon flux is given by $N_i\sigma_A(\omega_s, \omega_i)$. Hence we obtain

$$N_s = (N_i - 1) + N_i\sigma_A(\omega_s, \omega_i). \tag{7.45b}$$

Time-reversal symmetry requires that the number of photons N_s emerging from the medium after time reversal (Fig. 7.19b) be equal to the number of in-coming photons N_i before reversal (Fig. 7.19a). Therefore

$$N_i = (N_i - 1) + N_i\sigma_A(\omega_s, \omega_i) \tag{7.46a}$$

or

$$1 = N_i\sigma_A(\omega_s, \omega_i). \tag{7.46b}$$

Since we have chosen N_i to be $1/\sigma(\omega_s, \omega_i)$ in (7.45a), we obtain from (7.46b)

$$\sigma(\omega_i, \omega_s) = \sigma_A(\omega_s, \omega_i). \tag{7.47}$$

From (7.47) we can go back to $\mathcal{R}$ to show that the *Stokes* Raman tensor element for incident photon frequency ω_i and incident and scattered photons polarizations equal to $\boldsymbol{e}_i$ and $\boldsymbol{e}_s$, respectively, is equal to the corresponding *anti-Stokes* tensor element for incident photon frequency ω_s and incident and scattered photon polarizations equal to $\boldsymbol{e}_s$ and $\boldsymbol{e}_i$, respectively. If

we neglect the difference between ω_i and ω_s, there is no distinction between Stokes and anti-Stokes scattering and the Raman tensor is *symmetric* with respect to an interchange between $\boldsymbol{e}_i$ and $\boldsymbol{e}_s$. The equality between the Stokes scattering cross section $\sigma(\omega_i, \omega_s)$ and the corresponding anti-Stokes scattering cross section $\sigma_{AS}(\omega_s, \omega_i)$ has been tested directly in GaAs multiple quantum wells (see Sect. 9.2.4 for further description of the optical properties of these quantum wells) under resonance condition (see Sect. 7.2.8 on the meaning of resonant Raman scattering) where both the Stokes and anti-Stoke scattering cross sections are strongly dependent on the incident photon energy [7.60]. Readers interested in the application of (7.47) to measure phonon occupancy and temperature should download the webpage **http://Pauline.Berkeley.edu/textbook/PhononOccupancy.pdf**.

7.2.3 Experimental Determination of Raman Spectra

a) Experimental Techniques

The measurement of a Raman spectrum requires at least the following equipment:

- a source of collimated and monochromatic light;
- an efficient optical system to collect the weak scattered radiation;
- a spectrometer to analyze the spectral content of the scattered radiation and
- a highly sensitive detector for the scattered radiation.

Since Raman efficiencies are typically very small (in some cases as small as 10^{-12}), every component in this system has to be optimized. We shall now consider these components individually.

Light Source

In the days before the advent of lasers, the light source was typically a high power discharge lamp. Discrete emission lines of a gas or vapor (typically mercury vapor) were used. In those days only transparent samples could be studied because of their larger scattering lengths. Since many common semiconductors are opaque, Raman studies of semiconductors became feasible only after the advent of lasers. High power pulsed lasers, such as the ruby laser which appeared first, made it possible to observe *stimulated Raman scattering* (see, for example, [7.61]). However, they are not well suited for studying spontaneous Raman scattering for which a continuous wave (cw) laser of high time-averaged power is preferred. As a result the cw He-Ne laser (wavelength $\lambda = 632.8$ nm) was the first laser to be used in Raman scattering. But soon it was replaced by the Nd:YAG, Ar^+ and Kr^+ ion lasers. The latter two produce several high power (> 1 W in a single line) discrete emission lines covering the red (647 nm), yellow (564 nm), green (514 nm), blue (488 nm) and violet (458 nm) regions of the visible spectrum. With these high average power

cw lasers it became feasible to obtain not only one-phonon Raman spectra in semiconductors but also their two-phonon spectra. With continuously tunable cw lasers based on dyes (1 μm $\geq \lambda \geq$ 450 nm), color-centers in ionic crystals (3 μm $\geq \lambda \geq$ 1 μm) and more recently Ti-doped sapphire (1 μm $\geq \lambda \geq$ 700 nm) it became possible to perform *Raman excitation spectroscopies*, i. e., resonant Raman scattering. In analogy to the luminescence excitation spectroscopy discussed in Sect. 7.1.5, in resonant Raman spectroscopy one monitors the Raman efficiency as a function of the excitation laser wavelength. The physics involved in this kind of spectroscopy will be discussed in Sect. 7.2.7.

Spectrometers

In most Raman experiments on semiconductors the signal is 4–6 orders of magnitude weaker than the elastically scattered laser light. At the same time the difference in frequency between the Raman signal and the laser light is only about 1% of the laser frequency. In order to observe this weak sideband in the vicinity of the strong laser light, the spectrometer must satisfy several stringent conditions. First it must have good *spectral resolving power*. Modern Raman spectrometers typically have resolving power $(\lambda/\Delta\lambda) > 10^4$, which can be obtained easily with diffraction gratings. It is, however, important that these gratings do not produce "ghosts" and "satellites", which can be confused with Raman signals. Modern holographic gratings (Sect. 6.1.2) have practically eliminated this problem. A Raman spectrometer must also have an excellent *stray light rejection ratio*. This is defined as the ratio of the background stray light (light at all wavelengths other than the nominal one specified by the spectrometer) to the signal. Stray light is produced by imperfections in the optics (such as mirrors and gratings) and by scattering of light off walls and dust particles inside the spectrometer. Most spectrometers have a rejection ratio of 10^{-4}–10^{-6}. As a result, the background stray light can be orders of magnitude larger than the Raman signal. This situation can be solved by: (a) making the sample surface as smooth as possible to minimize the elastically scattered laser light; (b) using a "notch filter", which will block out the laser light; (c) putting two or more spectrometers in series. A properly designed *double monochromator* can have rejection ratios as small as 10^{-14}, equal to the product of the ratios for the two monochromators. This rejection ratio is adequate for Raman studies in most semiconductors. Nowadays *triple spectrometers* have become popular for use with **multichannel detectors** to be described next. In these spectrometers two monochromators are put "back-to-back" for use as a notch filter. The *third monochromator* provides all the dispersion required for separating the Raman signal from the laser light.

Detector and Photon-Counting Electronics

Raman recorded the weak inelastically scattered light in his pioneering experiment in 1928 by using photographic plates. These detectors actually have many of the desirable characteristics of modern systems. They have the sensitivity to detect individual photons. They are *multichannel detectors* in that

they can measure many different wavelengths at the same time. Finally, they can integrate the signal over long periods of time, from hours to even days. They also have one big advantage compared to modern detector systems: they are inexpensive! However, they also have some serious drawbacks: Their outputs are not linear in the light intensity and it is also cumbersome to convert the recorded signal into digital form for analysis. The first major advance in photoelectric recording (see Chap. 8 for discussions of the photoelectric effect) of Raman spectra was the introduction of *photon counting* methods [7.62]. Instead of integrating all the photocurrent pulses arriving at the photomultiplier tube anode as the signal, a *discriminator* selects and counts only those pulses with large enough amplitude to have originated at the photocathode. The background pulses (noise) remaining in such systems are those generated by thermionic emission of electrons at the photocathode. This can be minimized by cooling the entire photomultiplier tube to about −20C (via thermoelectric coolers) or to liquid nitrogen temperature. One of the most popular photomultipliers for Raman scattering has a GaAs photocathode cooled to −20C. When coupled to properly designed counting electronics, such a detector system has a background noise (or *dark counts*) of a few counts per second and a *dynamic range* of 10^6.

The above detector system has one major disadvantage compared with the photographic plate. It counts the total number of photons emerging from the spectrometer without spatially resolving the positions (and hence the wavelengths) of the photons. As a result, the Raman spectrum is obtained only after scanning the spectrometer output over a wavelength range containing the Raman peak. Recently several multichannel detection systems have become available commercially. These systems are based on either *charge-coupled devices* (CCDs) or *position-sensitive imaging photomultiplier tubes*. These detectors have been reviewed by *Chang* and *Long* [7.63] and by *Tsang* [7.64]. The CCD detector is essentially the same as a modern television camera. Its sensitivity can be enhanced by adding an image-intensifier tube. This tube consists of a photocathode as in a photomultiplier tube. The photoelectrons generated at the cathode are multiplied by a factor of 10^6–10^7 through a *microchannel plate*. This is essentially a honeycomb consisting of many tiny glass tubes whose interior walls are coated with a secondary electron emitter. Just one such glass tube with an enlarged entrance in the shape of a funnel is known as a *channeltron* (see Fig. 8.9 for a sketch). A high voltage is applied between the entrance and exit ends of each glass tube. When an electron enters the tube and hits the secondary emitter wall it generates several additional electrons. These will, in turn, produce more secondary electrons when they impact the glass wall. Thus an "avalanche" of secondary electrons is created as they travel down the narrow tube. A phosphor at the exit end of the microchannel plate converts the electron pulses back into a brighter image.

An imaging photomultiplier tube [7.65, 66] (also known as a *Mepsicron*) has essentially the same construction as an image-intensifier tube except that the phosphor is replaced by an anode with four output leads (Fig. 7.20). When

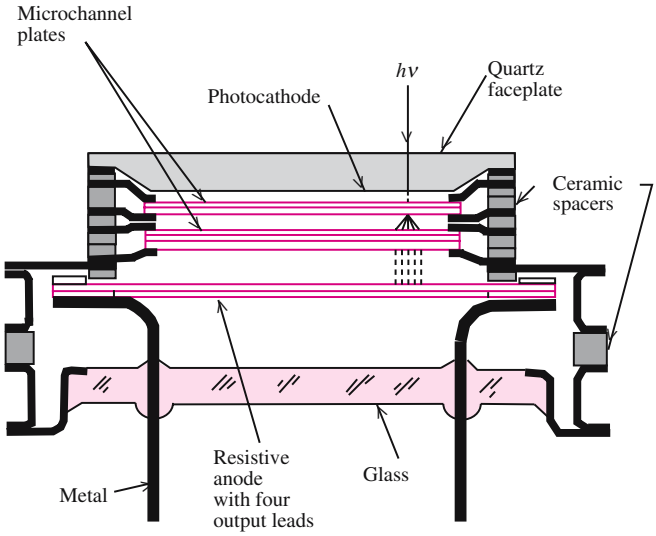

Fig. 7.20. Schematic diagram of the construction of a position-sensitive imaging photomultiplier tube

an amplified electron pulse hits the anode, it generates four electrical output pulses from these four anode leads. Depending on the position of the electron pulse on the anode, these four output pulses emerge at different times. A timing circuit measures the arrival time delays between these four pulses. An analog computer calculates the position of the original electron pulse at the anode based on these time delays. This detector has all the advantages of a photomultiplier tube plus a much lower dark count. Since each pixel is equal to one "channel" and the area of a pixel is much smaller than a photomultiplier tube, its dark current per channel is also much smaller. The dark current of a cooled imaging tube can be as low as 0.01 counts/second per channel. The major disadvantage of this detector is its finite lifetime. Every time a photoelectron is amplified by the microchannel plate positive ions are emitted in the channel plates and accelerated towards the photocathode. As a result, such detectors are rated to have a total lifetime of 10^{13} photoelectrons/pixel. Obviously, such detectors should be used only for extremely weak signals. For obvious reasons the dynamical range of the mepsicrons is small, typically $< 10^5$ electrons/pixel. The relative merits of the CCD and the Mepsicron multichannel detection systems have been compared by *Tsang* [7.64].

b) Experimental Phonon Raman Spectra in Semiconductors

One-Phonon Raman Spectra

Figure 7.21 shows Raman spectra of several group III–V semiconductors (GaAs, InP, AlSb) measured by *Mooradian* and *Wright* [7.67] using a Nd:YAG laser (1.06 μm wavelength) as the excitation source in a 90° scattering geometry (note

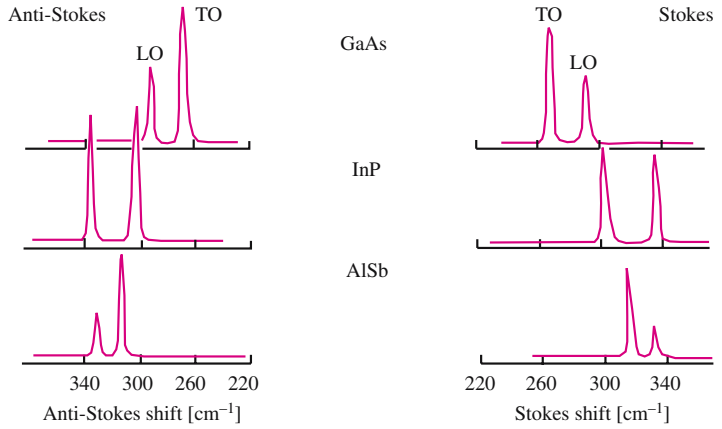

Fig. 7.21. Raman spectra of three zinc-blende-type semiconductors showing the TO and LO phonons in both Stokes and anti-Stokes scattering. Note that the vertical scales are not the same for all spectra. (From [7.67])

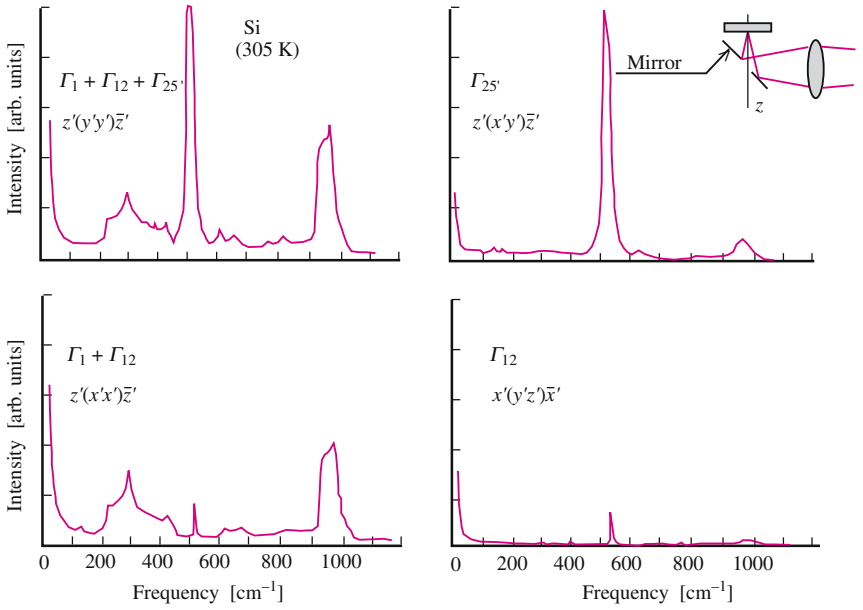

Fig. 7.22. First (peak at 520 cm^{-1}) and second order Raman spectra of Si obtained in the scattering geometry shown in the *inset*. The notations for the scattering configuration in each spectrum are defined in Sect. 7.2.2. (From [7.68])

that these semiconductors are transparent to this wavelength). In this geometry both the TO and LO phonons are allowed by the selection rules discussed in Sect. 7.2.2. Figure 7.22 shows the Raman spectra of Si obtained by *Temple* and *Hathaway* [7.68] in backscattering geometry but with several different

polarization configurations. These configurations allowed them to extract components of the Raman tensor with different symmetries. Notice that there is only one very strong one-phonon peak at 519 cm^{-1} (at 305 K), corresponding to the zone-center optical phonons in Si (the TO and LO phonons are degenerate at zone center in diamond-type crystals as pointed out in Sect. 3.1). In agreement with selection rules, this peak appears only in scattering configurations where the $\Gamma_{25'}$ components of the Raman tensor are allowed. It appears rather weakly in the "forbidden" configurations; it is easy to figure out possible reasons (e. g., imperfect polarizers).

Two-Phonon Raman Spectra

In addition to the one-phonon peak, *Temple* and *Hathaway* also observed a number of weaker structures, which were identified with two-phonon Raman scattering. While the selection rules for two phonon-scattering in semiconductors are beyond the scope of this book, they have been studied by several researchers [7.69, 70]. In Si, components of the two-phonon Raman tensor with symmetries $\Gamma_{25'}$, Γ_{12} and Γ_1 are allowed. Notice that the two-phonon spectra show peaks and shoulders that are reminiscent of structures in the three-dimensional density of states associated with critical points. This is not surprising since, as we pointed out in Sect. 7.2.1, overtone two-phonon Raman spectra mimic the phonon density of states. The two-phonon Raman peaks in Si roughly fall into three groups (similar results are found in zinc-blende-type semiconductors although the phonon frequencies may be different). The broad low-energy peak in the range of 200–450 cm^{-1} in Fig. 7.22 is the result of overtone scattering from the acoustic phonons. The few bands near the one-phonon peak are combination modes involving one optical phonon and one acoustic phonon. Finally, the high-energy peak located between 900 and 1000 cm^{-1} is due to overtone scattering by two optical phonons. Figure 7.23 shows the two-phonon Raman spectrum in Ge obtained by *Weinstein* and *Cardona* [7.71]. In order to compare the two-phonon Raman spectrum with the experimental phonon density of states (deduced from neutron scattering results), these researchers took the linear combination $\Gamma_1 + 4\Gamma_{12}$ of the two-phonon Raman spectra and then divided it by the factor $[N(\omega) + 1]^2$ [where $N(\omega)$ is the Bose–Einstein occupation number of the phonon mode with frequency ω] to eliminate the effect of phonon occupation number. The resultant "reduced" two-phonon spectrum is the solid curve in Fig. 7.23. This is compared with the two-phonon "overtone" density of states (broken curve) obtained from the one-phonon density of states curve based on the phonon dispersion curves of Ge [7.72] but with the phonon frequency doubled. Except for the strong, sharp one-phonon peak at around 300 cm^{-1} in the experimental spectrum (which could not be completely eliminated because of imperfect polarizers), the agreement between the two curves is quite good, especially in the two-acoustic-phonon part of the spectrum. The vertical bars and labels in this figure highlight the critical points in the Brillouin zone [numbers in parentheses denote the phonon branches, counting from lower (TA) to higher (TO)

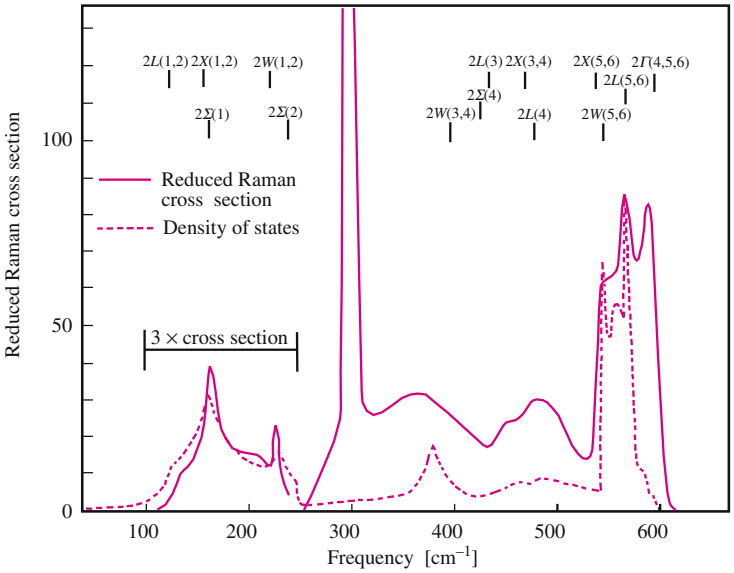

Fig. 7.23. "Reduced" two-phonon Raman spectrum of Ge compared with the density of two-phonon overtone states. The experimental two-phonon Raman spectrum containing the components with symmetry $\Gamma_1 + 4\Gamma_{12}$ has been divided by the factor $[N(\omega) + 1]^2$, where $N(\omega)$ is the Bose–Einstein occupation number of the phonon mode with frequency ω. (From [7.71]). Note that at low frequencies the reduced Raman cross section lies below the density of states (see Problem 7.15)

frequencies] which contribute to the structures in the two-phonon "overtone" density of states.

Raman Spectra of Semiconductor Monolayers

The development of high intensity laser sources for Raman spectroscopies has made it possible to measure the Raman spectra of opaque semiconductors. Still the thickness of sample probed is of the order of the optical penetration depth, which is typically larger than 100 nm. With the appearance of optical multichannel detectors it is now possible to measure the Raman spectra of monolayers of semiconductor materials. Figure 7.24c shows the Raman spectrum of two monolayers of Ge deposited on a Si(100) substrate. It is obtained by subtracting the spectrum of the Si substrate (Fig. 7.24a) from that of the Ge layer plus the Si substrate (Fig. 7.24b). Compared with the Raman spectrum of bulk Ge, the Ge monolayer shows one extra peak at 410 cm^{-1}. Figure 7.25 shows the thickness dependence of the Raman spectra of Ge monolayers on Si(100) substrates. For comparison, Fig. 7.25d shows the Raman spectrum of a bulk Ge-Si alloy. These spectra indicate that the 410 cm^{-1} peak is also present in the bulk Ge-Si alloy. It is strongest in the two-monolayer Ge film. As the Ge film thickness increases, the intensity of this peak decreases rel-

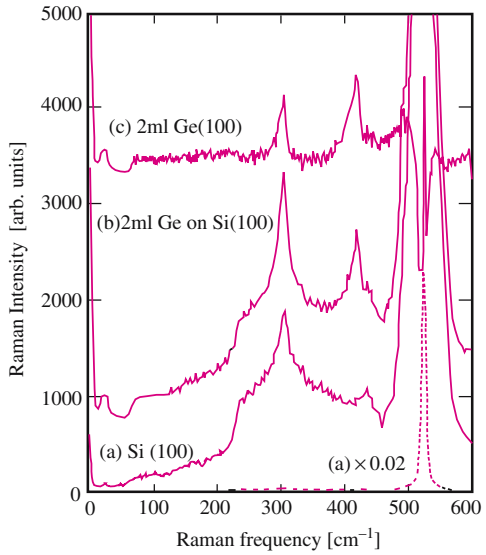

Fig. 7.24. Raman spectrum (*c*) of two monolayers of Ge deposited on a Si(100) substrate obtained by subtracting spectrum (*a*) from (*b*). (From [7.64])

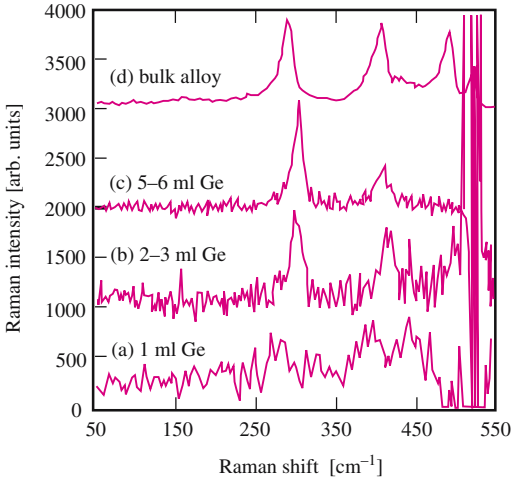

Fig. 7.25. Evolution of Raman spectra of monolayers of Ge deposited on a Si(100) substrate and then protected by 10 nm of Si as a function of Ge layer thickness. These spectra have been obtained in the same way as those in Fig. 7.24. Spectrum (*d*) is that of a bulk Ge-Si alloy. (From [7.64])

ative to that of the bulk Ge TO Raman peak at 300 cm^{-1}. All these properties are consistent with the interpretation that this 410 cm^{-1} peak is associated with the vibration of a Ge-Si bond that forms at the interface between the Ge monolayer and the Si substrate. These results emphasize the power of Raman spectroscopy for characterizing semiconductor systems.

Raman Spectra of Phonon-Polaritons

Usually the phonon wavevector observed by Raman scattering in semiconductors is too small to be used for mapping out the phonon dispersion over